certainties of probe-pattern parasitics and device capacitances determined from the previous cutoff technique, due to cutoff biasing, are eliminated by the optimization of HBTs in the active mode. The remainder of the device parameters are determined from the active mode optimization. The HBT equivalent circuit including a RF probe pad and interconnection circuit model determined from these techniques shows good agreement with measured S-parameters, while providing physically acceptable circuit parameter values. The extrinsic device de-embedded from probe-pattern parasitics may be used in circuit design programs.

ACKNOWLEDGMENT

The authors would like to thank B. J. Moon and Z. Abid for helpful discussions.

REFERENCES

[1] D. Costa, W. Liu, and J. S. Harris, Jr., "A new direct method for determining the heterojunction bipolar transistor equivalent circuit model," in *Proc. 1990 IEEE Bipolar Circuits and Technology Meeting*, pp. 118–121.

[2] M. E. Kim, A. K. Oki, J. B. Camou, P. D. Chow, B. L. Nelson, D. M. Smith, J. C. Canyon, C. C. Yang, R. Dixit, and B. R. Allen, "12–40 GHz low harmonic distortion and phase noise performance of GaAs heterojunction bipolar transistors," in *1988 IEEE GaAs IC Symp. Dig.*, pp. 117–120.

[3] B. Bayraktaroglu, and R. D. Hudgens, M. A. Khatibzadeh, and H. Q. Tserng, "2.5 W CW X-Band heterojunction bipolar transistor," in *1989 IEEE MTT-S Int. Microwave Symp. Dig.*, pp. 1057–1060.

[4] B. Bayraktaroglu, N. Camilleri, and S. A. Lambert, "Microwave performances of n-p-n and p-n-p AlGaAs/GaAs heterojunction bipolar transistors," *IEEE Trans. Microwave Theory Tech.*, vol. 36, pp. 1869–1873, 1988.

[5] U. K. Mishra, J. F. Jensen, D. B. Rensch, A. S. Brown, W. E. Stanchina, R. J. Trew, M. W. Pierce, and T. V. Kargodorian, "Self-aligned AlInAs-GaInAs heterojunction bipolar transistors and circuits," *IEEE Electron Device Lett.*, vol. 10, pp. 467–469, 1989.

[6] R. J. Trew, U. K. Mishra, and W. L. Pribble, "A parameter extraction technique for heterojunction bipolar transistors," in *1989 IEEE MTT-S Int. Microwave Symp. Dig.*, pp. 897–900.

[7] G. L. Bilbro, M. B. Steer, R. J. Trew, C. R. Chang, and S. G. Skaggs, "Extraction of the parameters of equivalent circuits of microwave transistors using tee annealing," *IEEE Trans. Microwave Theory Tech.*, vol. 38, pp. 1381–1390, 1990.

[8] P. J. van Wijnen, H. R. Claessen, and E. A. Wolsheimer, "A new straightforward calibration and correction procedure for "On wafer" high frequency S-parameter measurements (45 MHz–18 GHz)," in *Proc. 1987 IEEE Bipolar Circuits and Technology Meeting*, pp. 70–73.

[9] S. Lee and A. Gopinath, "New circuit model for RF probe pads and interconnections for the extraction of HBT equivalent circuit," *IEEE Electron Device Lett.*, vol. 12, pp. 521–523, 1991.

[10] F. Diamant and M. Laviron, "Measurement of the extrinsic series elements of a microwave MESFET under zero current condition," in *Proc. 12th European Microwave Conf.*, 1982, pp. 451–456.

[11] W. R. Curtice and R. L. Camisa, "Self-consistent GaAs FET models for amplifier design and device diagnostics," *IEEE Trans. Microwave Theory Tech.*, vol. MTT-32, pp. 1573–1578, 1984.

[12] M. I. Nathan, W. P. Dumke, K. Wrenner, S. Tiwari, S. L. Wright, and K. A. Jenkins, "Electron mobility in p-type GaAs," *Appl. Phys. Lett.*, vol. 52, pp. 654–656, 1988.

[13] H. H. Lin and S. C. Lee, "Super-gain AlGaAs/GaAs heterojunction bipolar transistor using an emitter edge-thinning design," *Appl. Phys. Lett.*, vol. 47, pp. 839–841, 1985.

[14] *EEsof Touchstone Reference Manual*, version 1.7, EEsof Inc., 1989.

[15] W. M. C. Sansen and R. G. Meyer, "Characterization and measurement of the base and emitter resistances of bipolar transistor," *IEEE J. Solid-State Circuits*, vol. SC-7, pp. 492–498, 1972.

[16] S. M. Sze, *Physics of Semiconductor Devices*, 2nd ed. New York: Wiley, 1981, pp. 33.

[17] M. B. Das, "High-frequency performance limitations of millimeter-wave heterojunction bipolar transistors," *IEEE Trans. Electron Devices*, vol. 35, pp. 604–614, 1988.

[18] I. E. Getreu, *Modeling the Bipolar Transistor*. Amsterdam: Elsevier, 1978, pp. 140–143.

[19] A. Neugroschel, "Measurement of the low-current band and emitter resistances of bipolar transistors," *IEEE Trans. Electron Devices*, vol. 34, pp. 817–822, 1987.

An Analysis of a Coupled-Ring Rotary Joint Design

E. D. Evans

***Abstract*—This paper describes a theoretical and experimental analysis of a coupled-ring rotary joint design. A rotary joint of this type is commonly used for mechanically scanned, multichannel radars. The main goal of the analysis is to develop a better understanding for the transfer of energy through the joint's highly coupled rings. We first consider the geometry of a typical single channel and then describe a coupled transmission line model for the coupled-ring network. Using the model, we determine the type of ring network needed for low channel loss and small rotational variations of this loss. A series of measurements on some test models support the predictions of the analysis.**

I. INTRODUCTION

Many radar systems use multichannel rotary joints to allow mechanical scanning of the radar beam in azimuth or elevation. More recent radar designs require rotary joints with higher powers and larger numbers of channels to achieve new range and beamforming requirements. Because of these new requirements, multichannel rotary joints must be carefully designed to achieve low channel loss and small rotational variations of this loss.

In this paper a theoretical model for the performance of a coupled-ring rotary joint is derived. This type of rotary joint is commonly used in radars that have more than five or six channels. The theoretical approach uses coupled transmission line theory to model the transfer of energy across the joint's highly coupled rings. Using the model, we calculate the effect of the coupled-ring network on the joint's power transmission coefficient. To check the predictions of the theory, we also measure the performance of some rotary joint test models.

Fig. 1 shows a cross section view and an expanded three-dimensional view of a typical coupled-ring rotary joint channel. The single channel consists of a stationary stator section and a rotating rotor section. The channel has a pancake shape that can be stacked for multichannel systems, and the ring design allows a hole through the center of the joint for passing cables to the multiple channels. The key components of the single channel are the stator and rotor coupling rings. The rings sit in a ring cavity and are positioned very closely together to allow strong capacitive coupling. The circumference of the rings is usually under a wavelength, and the size of the ring cavity is small enough to prevent the propagation of any coaxial waveguide modes.

Manuscript received July 13, 1990; revised August 15, 1991. This work is supported by the Department of the Navy under Air Force Contract F19628-85-C-0002.

The author is with the MIT Lincoln Laboratory, 244 Wood Street, Lexington, MA 02173.

IEEE Log Number 9105447.

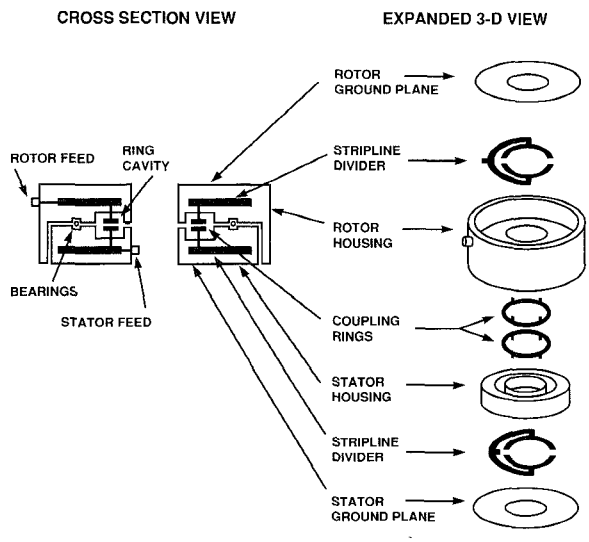

Fig 1. Cross section view and an expanded three dimensional view of a coupled-ring rotary joint design.

The energy traveling through a single rotary joint channel goes through several components of the rotor and stator. Energy traveling into the rotor feed is first divided equally by a stripline network. The network is typically a four-way or eight-way power divider consisting of cascaded, two-way Wilkinson dividers. The outputs of the divider are connected to a set of ring feeds spaced equally around the rotor ring. The feeds excite the rotor ring, and energy capacitively couples to the stator ring. An equal number of output feeds collects energy from the stator ring and sends it through a stripline combining network to the output stator feed. Usually the combining network is electrically identical to the stripline dividing network.

The ground path for the single channel is across the small gap between the rotor and stator housings. At microwave frequencies part of this gap can be set up as a quarter-wavelength choke to short the ground path gap in the ring cavity. At lower frequencies quarter-wavelength chokes are usually too long to fit in the housings, and small point contacts are used to short the ground path.

When the rotation angle of the rotor changes, the orientation between the rotor and stator ring feeds changes. The changes cause rotational variations in the phase and amplitude of the channel's transmission coefficient S_{21}. These variations are called the S_{21} wow, and they are usually measured in units of S_{21} dB per degree of rotation and S_{21} degrees per degree of rotation. The value of the S_{21} wow can have a significant effect on a radar's MTI and adaptive nulling performance.

To investigate the effect of the ring network on a single channel's power transmission coefficient, it is useful to have a good theoretical model for the network. In this paper we derive a theoretical model for the ring network and test it through a series of measurements. Using the model, we investigate the effects of the ring cavity impedances, ring circumference, and feed spacing on the value of S_{21}.

Some previous authors have considered the performance of other types of rotary joints. The earliest work [1] describes the design of single channel waveguide and coaxial rotary joints. In [2]–[5], several types of annular waveguide rotary joints are described. These types of joints are adequate for use in high-power multichannel radars, but they all tend to be very large in size at L-band and UHF frequencies. In [6] and [7], multichannel coaxial joints are described for S-, C- and X-band systems. In [8] a brief review of several single channel and multichannel rotary joints is given. The paper mentions a coupled-ring design, but gives no detailed analysis.

In Section II of this paper, we first describe a coupled transmission line model for the coupled-ring network. We calculate S_{21} for a single-input/single-output ring network as a function of its even- and odd-mode impedances and ring circumference. In Section III we find the best coupled-ring impedances and feed spacing for a good match between the rings and feeds. The analysis also gives the theoretical S_{21} wow performance for the coupled-ring design.

II. Models for the Coupled-Ring Network

Fig. 2(a) shows an equivalent transmission line circuit for a coupled-ring network. For this network four input feeds are spaced equally around the upper transmission line ring, and four output feeds spaced equally around the lower transmission line ring. The input and output feeds are offset by an arbitrary rotation angle. The fields between the transmission line rings are highly coupled to allow an efficient transfer of energy between the input and output feeds. To simplify the sketch, the ground paths have not been shown.

The symmetries in Fig. 2(a) suggest a way to simplify the network and break the ring into smaller equivalent rings. For a symmetric and balanced input and output feed system, the ring voltages and currents at an angle θ have the same value as the ring currents and voltages at angles $\theta + 90°$, $\theta + 180°$, and $\theta + 270°$. Because of this equivalence of voltages and currents, we can break the ring at these symmetry points and recombine a ring section into a smaller ring with a single input feed and a single output feed. The smaller ring shown in Fig. 2(b) has the same power transmission properties as the ring in Fig. 2(a), except that the wow variations of S_{21} are modulo 360° for the small ring and modulo 90° for the large ring.

Fig. 3 shows a more detailed sketch of the ring network from Fig. 2(b). The figure shows that the coupled-ring network is a parallel combination of two coupled-line sections, labeled section A and section B. Each of these coupled-line sections has a four-port network equation written in terms of y parameters. For symmetric and lossless coupled lines, the voltages and currents at the four ports are related by [10]

$$\begin{bmatrix} I_1 \\ I_2 \\ I_3 \\ I_4 \end{bmatrix} = \begin{bmatrix} y_{11} & y_{12} & y_{13} & y_{14} \\ y_{21} & y_{22} & y_{23} & y_{24} \\ y_{31} & y_{32} & y_{33} & y_{34} \\ y_{41} & y_{42} & y_{43} & y_{44} \end{bmatrix} \begin{bmatrix} V_1 \\ V_2 \\ V_3 \\ V_4 \end{bmatrix}, \tag{1}$$

where

$$y_{11} = y_{22} = y_{33} = y_{44} = -j \frac{(1/Z_{0o} + 1/Z_{0e})}{2} \cot(\beta l), \tag{2}$$

$$y_{12} = y_{21} = y_{34} = y_{43} = -j \frac{(1/Z_{0o} - 1/Z_{0e})}{2} \cot(\beta l), \tag{3}$$

$$y_{13} = y_{31} = y_{24} = y_{42} = -j \frac{(1/Z_{0o} - 1/Z_{0e})}{2} \csc(\beta l), \tag{4}$$

$$y_{14} = y_{41} = y_{23} = y_{32} = -j \frac{(1/Z_{0o} + 1/Z_{0e})}{2} \csc(\beta l). \tag{5}$$

In the above equations l is the length of the coupled-line system, and β is the propagation constant $2\pi/\lambda$.

In equations (2)–(5), Z_{0e} is the network's even-mode characteristic impedance, and Z_{0o} is the network's odd-mode impedance.

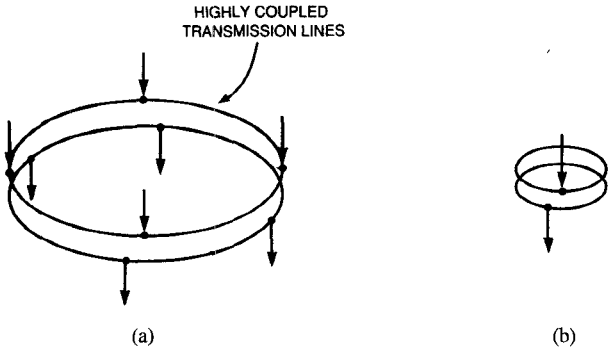

Fig. 2. Equivalent coupled transmission line models for a coupled-ring system.

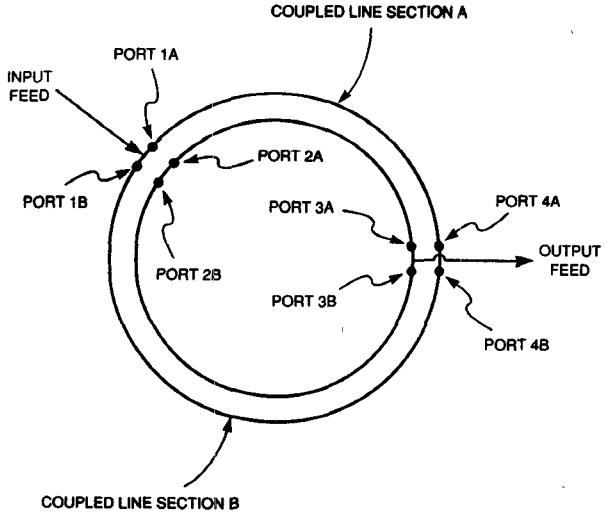

Fig. 3. Coupled transmission line model for a single-input/single-output coupled-ring network. The ground paths have been omitted to simplify the drawing.

Simple expressions for these impedances are written [11]

$$Z_{0e} = \frac{1}{vC_0}, \tag{6}$$

$$Z_{0o} = \frac{1}{v}\left(\frac{1}{C_0 + 2C_m}\right), \tag{7}$$

where v is the propagation velocity for the even and odd modes, C_0 is the capacitance between a single line and ground (with the other line present), and C_m = is the coupling capacitance between the two lines. For a set of highly coupled lines, Z_{0e} depends mainly on the fields around the coupled lines, and Z_{0o} depends mainly on the fields between the two lines.

To find the transmission coefficient for the ring network in Fig. 3, we next calculate the y and z parameters for the total network. The y parameter expressions for each coupled-line section are written in the vector form

$$\boldsymbol{I}_A = \boldsymbol{Y}_A \boldsymbol{V}_A, \tag{8}$$

$$\boldsymbol{I}_B = \boldsymbol{Y}_B \boldsymbol{V}_B, \tag{9}$$

where $\boldsymbol{Y}_A$ is the y parameter matrix for the coupled-line section A, and $\boldsymbol{Y}_B$ is the y parameter matrix for the coupled-line section B. When the two networks are combined in parallel, the total voltage and current vectors are related by

$$\boldsymbol{I}_{\text{tot}} = \boldsymbol{Y}_A \boldsymbol{V}_A + \boldsymbol{Y}_B \boldsymbol{V}_B = \boldsymbol{Y}_{\text{tot}} \boldsymbol{V}_{\text{tot}}, \tag{10}$$

where $\boldsymbol{V}_{\text{tot}} = \boldsymbol{V}_A = \boldsymbol{V}_B$, and $\boldsymbol{Y}_{\text{tot}}$ is the y parameter network for the total network.

To solve for the input impedance of the network, we use

$$\boldsymbol{V}_{\text{tot}} = \boldsymbol{Y}_{\text{tot}}^{-1} \boldsymbol{I}_{\text{tot}} = \boldsymbol{Z}_{\text{tot}} \boldsymbol{I}_{\text{tot}}, \tag{11}$$

where $\boldsymbol{Z}_{\text{tot}}$ is the z parameter matrix for the total network.

The ring network in Fig. 3 is fed at ports 1 and 3, while ports 2 and 4 are left open. Since ports 2 and 4 are open, the currents $I_{2,\text{tot}} = I_{4,\text{tot}} = 0$, and the expressions for $V_{1,\text{tot}}$ and $V_{3,\text{tot}}$ are written

$$V_{1,\text{tot}} = z_{11,\text{tot}} I_{1,\text{tot}} + z_{13,\text{tot}} I_{3,\text{tot}}, \tag{12}$$

$$V_{3,\text{tot}} = z_{31,\text{tot}} I_{1,\text{tot}} + z_{33,\text{tot}} I_{3,\text{tot}}. \tag{13}$$

If port 1 is an input feed and port 3 is an output feed with load Z_L, the impedance looking into port 1 is written

$$Z_{\text{in}} = z_{11,\text{tot}} - \frac{z_{13,\text{tot}} z_{31,\text{tot}}}{(z_{33,\text{tot}} + Z_L)}. \tag{14}$$

The values of $|S_{21}|$ and $\angle S_{21}$ for the total network are calculated using (14) and the well known definitions given in [12].

III. Results

In this section we use the above ring network model to find the feed spacing and the values of Z_{0e} and Z_{0o} required for a good match and low S_{21} wow. For some of the results we compare calculated and measured values.

Fig. 4 shows a sketch of the coupled-ring model used for the measurements. The measurement model had a set of highly coupled stripline rings, centered between upper and lower ground planes. The stripline rings were separated by a thin dielectric sheet to allow strong capacitive coupling between them. To test the results of the calculations, the measurement model was set up with a single input feed and a single output feed, and both feeds had a $Z_0 = 50\ \Omega$. The ground plane spacing, stripline width, ring separation and cavity dielectric were then varied to create a wide range of even- and odd-mode impedances. To reduce the effects of the feed discontinuities, the measurements were made at low frequencies near 25 MHz. At these frequencies the rings in the measurement model were scaled to have a circumference near $\lambda/8$.

Fig. 5 shows the $|S_{21}|$ performance of the coupled-ring network as a function of Z_{0e}. For this case the input and output feeds are at the same orientation angle (the feeds are lined up), and the Z_{0o} has a value near 1 Ω. The figure shows that values of Z_{0e} between 160 and 360 Ω allow a good match between the feeds. Calculations and measurements for other feed orientations give similar results. Since large values of Z_{0e} require large ring cavities, the best values of Z_{0e} are probably between 160 and 200 Ω.

Fig. 6 shows the $|S_{21}|$ performance of the coupled-ring network as a function of ring circumference and Z_{0o}. The input and output feeds are again at the same orientation angle, and Z_{0e} has a value of 200 Ω. Fig. 6 shows that the network has the smallest transmission losses with a ring circumference between 0.05λ and 0.15λ. When the ring circumference is smaller than 0.05λ, the ring network performs more like a lumped capacitor, and the match is poor. When the ring circumference is larger than 0.150λ, the ring network performs more like a long stub tuner, and the match is again poor.

Fig. 6 also shows that the ring network performs well with Z_{0o} values smaller than 2 Ω. Knowing the largest acceptable value of

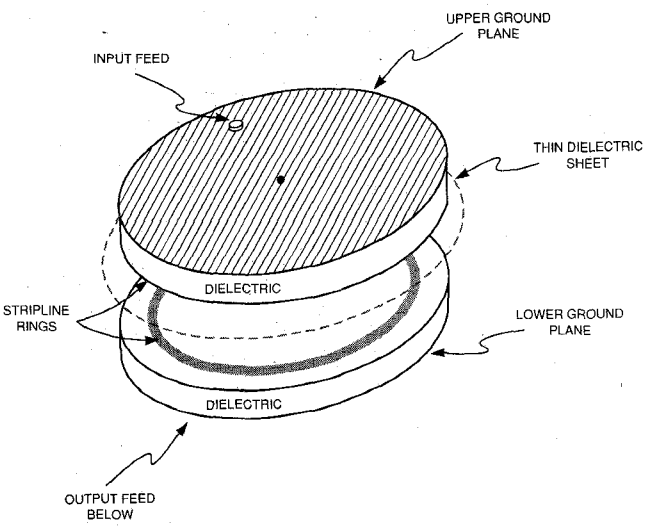

Fig. 4. Sketch of coupled-ring model for S_{21} measurements.

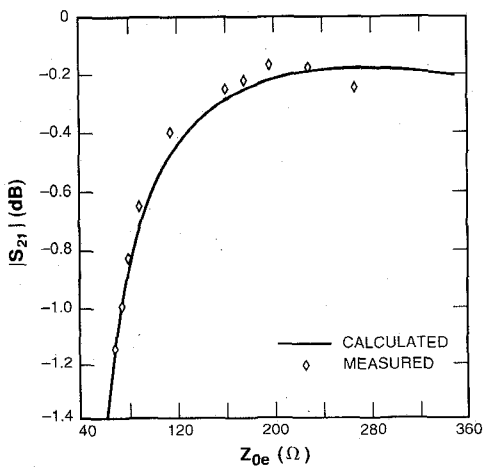

Fig. 5. $|S_{21}|$ versus Z_{0e} for the single-input/single-output coupled-ring network. The rotation angle between the input and output feeds is 0°.

Z_{0o} is important for the mechanical design of a channel. From (7) the value of Z_{0o} is inversely proportional to the capacitance between the rings. The impedance Z_{0o} is then proportional to the spacing between the rings. To avoid possible ring contact, it is important to choose the largest acceptable value of Z_{0o} and design the rings to be as far apart as possible.

Fig. 7 shows the peak-to-peak rotational variation of S_{21} as a function of ring circumference. This is equivalent to showing the peak-to-peak wow as a function of feed spacing for a multiple-input/multiple-output ring network. The wow values in the figure are for a well-matched ring network with $Z_{0e} = 200\ \Omega$ and $Z_{0o} = 1.0\ \Omega$. The figure shows that a ring circumference or feed spacing smaller than $\lambda/8$ allows relatively small values of $|S_{21}|$ and $\angle S_{21}$ wow.

Fig. 8 shows the relationship between S_{21} and the rotation angle between the feeds. For this case the ring network has $Z_{0e} = 200\ \Omega$, $Z_{0o} = 1.0\ \Omega$, and a ring circumference of $\lambda/8$. The value of $|S_{21}|$ (in dB) is most negative when the feeds are aligned, and least negative when the feeds are 180° opposite. The phase delay for the network is smallest when the feeds are aligned and largest when they are opposite. The differences in the S_{21} values for these feed orientations define the peak-to-peak wow for the coupled-ring network. Fig. 8 shows that the impedances and circumference chosen for the ring network allow a good match throughout the full range of rotation angles.

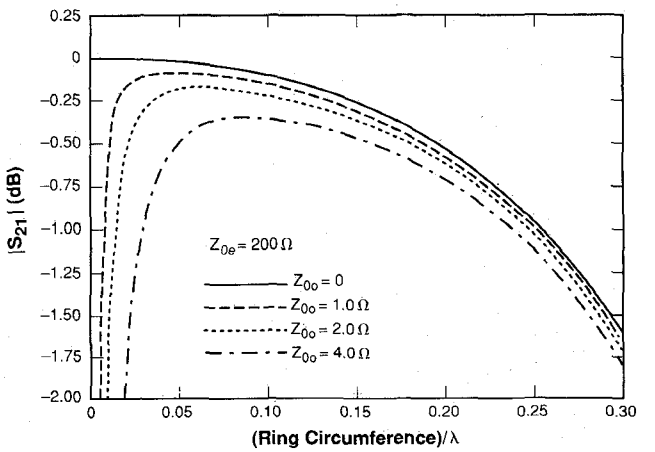

Fig. 6. Theoretical $|S_{21}|$ versus ring circumference and Z_{0o} for the case where $Z_{0e} = 200\ \Omega$. The rotation angle between the input and output feeds is 0°.

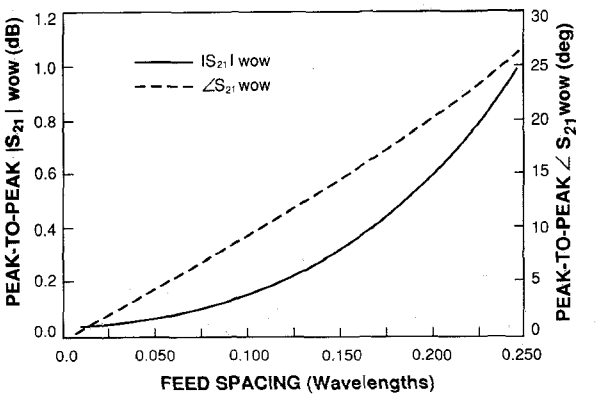

Fig. 7. Theoretical S_{21} wow as a function of feed spacing in wavelengths. For this case $Z_{0e} = 200\ \Omega$ and $Z_{0o} = 1.0\ \Omega$.

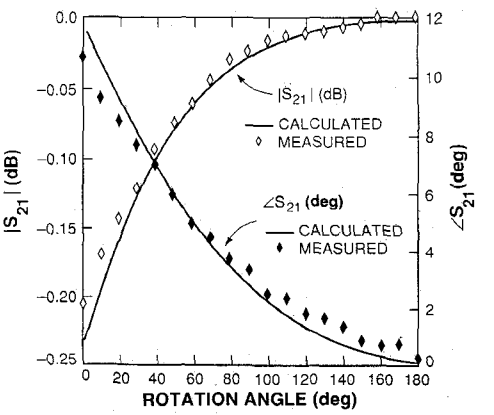

Fig. 8. Measured (after through calibration) and calculated S_{21} versus rotation angle for a well-matched coupled-ring model. For this case $Z_{0e} = 200\ \Omega$, $Z_{0o} = 1.0\ \Omega$, and the ring circumference is $\lambda/8$.

The measured values in Fig. 8 support the predictions of the theory. The measurements were taken after calibrating the network analyzer through the coupled-ring model. A through-calibration reduces the mismatch effects due to the feed-to-ring transitions.

Several techniques could be used to alter the S_{21} performance of a ring network. Using a mismatched ring network with stub tuners on the feeds is one possible narrowband approach to reduce wow. Reactive tuning networks near the feed-to-ring transitions can improve the wow performance in a similar way. Changing the relative phase and amplitude errors between the feeds in a multiple feed network also has an effect on wow. The effects of each of these techniques could be investigated in more detail using the approach outlined in this paper.

IV. Summary and Conclusion

In this paper a theoretical model for the performance of a coupled-ring rotary joint was derived. We first considered the configuration of a single channel and described a coupled transmission line model for the coupled-ring network. We then determined the type of ring network necessary for a good match and low wow variations. A series of measurements on some test models support the theoretical results.

The even-mode impedance, Z_{0e}; the odd-mode impedance, Z_{0o}; and the feed spacing have a significant effect on the transmission coefficient, S_{21}, for the coupled-ring network. For feed spacings between 0.05λ and 0.15λ, values of $160\ \Omega < Z_{0e} < 360\ \Omega$ and $Z_{0o} < 2\ \Omega$ give S_{21} values better than -0.3 dB. The size of the S_{21} wow variations can be controlled by changing the spacing between the ring feeds. Feed spacings less than $\lambda/8$ allow relatively small values of wow.

References

[1] G. L. Ragan, *Microwave Transmission Circuits*, MIT Radiation Laboratory Series, vol. 9, New York: McGraw-Hill, 1948, pp. 406–455.

[2] T. Tomiyasu, "A new annular waveguide rotary joint," *Proc. IRE*, vol. 44, pp. 548–553, Apr. 1956.

[3] W. E. Fromme, E. G. Fubini, and H. S. Keen, "A new microwave rotary joint," *Nat. Conv. Rev. IRE*, vol. 1, pp. 78–82, 1958.

[4] P. H. Smith and G. H. Mongold, "A high-power rotary waveguide joint," *IEEE Trans. Microwave Theory Tech.*, pp. 55–58, Jan. 1964.

[5] S. Boronski, "A multichannel waveguide rotating joint," *Microwave J.*, pp. 102–105, June 1965.

[6] E. W. Matthews and M. A. Ikemoto, "A multichannel rotary joint for spacecraft applications," *Nat. Conv. Rev. IRE*, vol. 1, pp. 157–159, 1968.

[7] M. Cohen, "A six-channel vertically stacked coaxial rotary joint for the S-, C-, and X-Band region," *Microwave J.*, pp. 71–74, Nov. 1964.

[8] H. S. Keen and A. J. Carini, "Multichannel rotary joints—How they work," *Microwaves*, vol. 3, no. 10, pp. 14–19, Oct. 1964.

[9] S. B. Cohn, "Coupled rectangular bars between parallel plates," *IRE Trans. Microwave Theory Tech.*, vol. 8, pp. 638–644, Nov. 1960.

[10] E. M. T. Jones, "Coupled strip transmission line filters and directional couplers," *IRE Trans. Microwave Theory Tech.*, vol. 4, no. 2, April 1956.

[11] L. N. Dworsky, *Modern Transmission Line Theory and Applications*. New York: Wiley Interscience, 1979, p. 114.

[12] R. E. Collin, *Foundations for Microwave Theory*. New York: McGraw-Hill, 1966, p. 177.

Computation of the Dispersion Characteristics of a Shielded Suspended Substrate Microstrip Line

I. P. Polichronakis and S. S. Kouris

Abstract—**The dispersion characteristics of a shielded suspended substrate microstrip line are calculated using five different sets of basis functions for the current distributions. Their comparison leads to the more suitable basis functions for the acquisition of fast and accurate results for frequencies up to 100 GHz.**

I. Introduction

Shielded suspended substrate microstrip lines (SSL) have been widely discussed in connection with the millimeter-wave integrated circuits [1]. Their electrical characteristics have been obtained using various methods of analysis [2]–[4]. In this paper the characteristics of the dominant mode for frequencies up to the millimeter wave region are determined using spectral domain analysis (SDA).

It is known that in the spectral domain method the assessment of the best basis functions for the current components on the strip is of fundamental importance for the numerical efficiency of the method; but it is also important to keep the computation time small enough. For this purpose a) the number of basis functions to approximate the actual current densities on the strip and b) the number of spectral terms necessary and sufficient to obtain an accurate solution for the effective dielectric constant (ϵ_{eff}) and the characteristic impedance (Z_0) of the line, must be considered and optimized. For this reason a number of sets of basis functions, found in the literature, are examined and their results are compared in order to find out the more suitable one which should be employed in the analysis of SSL.

II. Basis Functions

The characteristics of the dominant mode of the SSL, i.e., the characteristic impedance Z_0 and the effective dielectric constant $\epsilon_{\text{eff}} = (\beta/k_0)$, β being the propagation constant and k_0 the free-space wavenumber, are evaluated using the SDA as it is presented by Itoh [5] and Knorr and Tufekciogloy [6]. The cross-section of the SSL is illustrated in Fig. 1. In this work it is assumed that the line is lossless and the strip thickness is negligible.

It is well known that various sets of basis functions have been employed in the analysis of the different types of striplines. For instance, Itoh and Mittra used a first order approximation with a sine function for the representation of J_x and a triangular function for J_z [7]. Jansen proposed a full set of basis functions that ensures the singular behaviour of the field for any degree of solution accuracy and possesses the physical property of the surface current density to be twice differentiable [8]. Leung and Valanis [9] in order to obtain microstrip dispersion characteristics used also a first order solution. They adopted for the J_x current component the expression proposed by Delinger [10] and for the J_z current component the expression proposed by Kobayashi [11]. Other authors

Manuscript received February 25, 1991; revised July 22, 1991.

The authors are with Aristotelian University of Thessaloniki, Faculty of Engineering, School of Electrical Engineering, University P.O. Box 435, 54006 Thessaloniki, Greece.

IEEE Log Number 9105441.